Review

Real-Time Diffusion-Perfusion Mismatch Analysis in Acute Stroke

Matus Straka, PhD,[1,2] Gregory W. Albers, MD,[2,3] and Roland Bammer, PhD[1]*

Diffusion-perfusion mismatch can be used to identify acute stroke patients that could benefit from reperfusion therapies. Early assessment of the mismatch facilitates necessary diagnosis and treatment decisions in acute stroke. We developed the RApid processing of PerfusIon and Diffusion (RAPID) for unsupervised, fully automated processing of perfusion and diffusion data for the purpose of expedited routine clinical assessment. The RAPID system computes quantitative perfusion maps (cerebral blood volume, CBV; cerebral blood flow, CBF; mean transit time, MTT; and the time until the residue function reaches its peak, T_{max}) using deconvolution of tissue and arterial signals. Diffusion-weighted imaging/perfusion-weighted imaging (DWI/PWI) mismatch is automatically determined using infarct core segmentation of ADC maps and perfusion deficits segmented from T_{max} maps. The performance of RAPID was evaluated on 63 acute stroke cases, in which diffusion and perfusion lesion volumes were outlined by both a human reader and the RAPID system. The correlation of outlined lesion volumes obtained from both methods was $r^2 = 0.99$ for DWI and $r^2 = 0.96$ for PWI. For mismatch identification, RAPID showed 100% sensitivity and 91% specificity. The mismatch information is made available on the hospital's PACS within 5–7 min. Results indicate that the automated system is sufficiently accurate and fast enough to be used for routine care as well as in clinical trials.

Key Words: perfusion; diffusion; mismatch; acute stroke; automated data processing
J. Magn. Reson. Imaging 2010;32:1024–1037.

RECENT STUDIES SUGGEST that acute stroke patients with a significant mismatch between diffusion and perfusion lesion volumes on brain MRI are likely to benefit from reperfusion therapies (1,2). On the other hand, those with little or no mismatch as well as those with very large ischemic lesions may not benefit or may even be harmed (e.g., can suffer brain hemorrhage or reperfusion injury) following early reperfusion. Therefore, accurate and reliable diffusion-perfusion mismatch maps available in real-time is of great benefit to physicians who are treating acute stroke patients.

While perfusion and diffusion maps can be obtained separately with many software packages (3–5), there are only a few tools available to compute diffusion-perfusion mismatch maps (6–8). Moreover, currently available mismatch software relies heavily on user interaction, which is time-consuming and introduces operator-dependence into the results. Such complex software packages often require substantial training of stroke treatment team and operator errors are more than likely to occur. Overall, this poses significant disadvantages because immediate treatment of stroke patients is of utmost importance.

An ideal software package for routine diagnostic workup of acute stroke would (i) be fully automatic and operator-independent, (ii) generate maps of motion-corrected perfusion and diffusion parameters, (iii) determine diffusion-perfusion mismatch, (iv) provide maps and mismatch information no later than 5 min after the MRI scan, (v) be seamlessly integrated into existing clinical MR systems, (vi) output to a hospital's Picture Archiving and Communication System (PACS) and other communication devices, such as smartphones, for immediate review by the stroke treatment team, and (vii) deliver reliable processing results that are comparable to those generated by human observers.

In this study, we review common methods for diffusion-perfusion mismatch processing and present the RApid processing of PerfusIon and Diffusion (RAPID), which has been developed by our group during the last 3 years and is currently used on approximately 10 patients per day on a routine basis at our hospital. Specifically, we will introduce implementation details, compare results generated by human observers and the automated system, and provide a discussion

[1]Department of Radiology, Stanford University, Stanford, California, USA.
[2]Stanford Stroke Center, Stanford University Medical Center, Stanford, California, USA.
[3]Department of Neurology and Neurological Sciences, Stanford University, Stanford, California, USA.
Contract grant sponsor: NINDS; Contract grant number: R01NS39325; Contract grant sponsor: NIBIB; Contract grant number: R01EB2711; Contract grant sponsor: NIH; Contract grant number: 2R01 NS039325.
*Address reprint requests to: R.B., Department of Radiology, Stanford University, 1201 Welch Road, Lucas Center, Stanford, CA, 94305-5488. E-mail: rbammer@stanford.edu
Received March 31, 2010; Accepted August 2, 2010.
DOI 10.1002/jmri.22338
View this article online at wileyonlinelibrary.com.

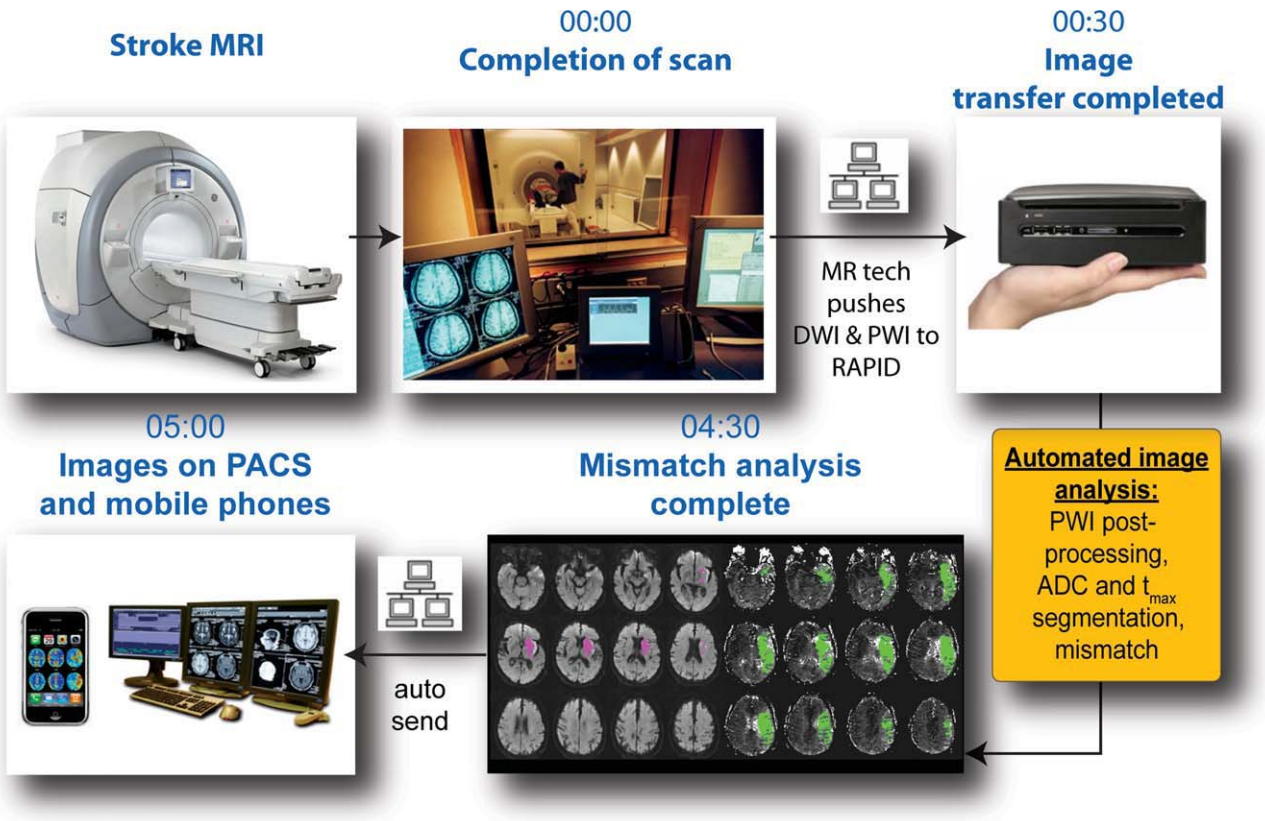

Figure 1. Basic scheme of the RAPID system workflow. After the diffusion and perfusion data are acquired, the scanner operator pushes the images over the network to a DICOM-compatible RAPID node. There, automatic processing is spawned and the resulting mismatch assessment and computation of PWI parameter maps are performed. Results are then available to hospital PACS, scanner console, email and smartphones in approximately 5–7 min. Color figure can be viewed in the online issue, which is available at wileyonlinelibrary.com.

about our initial experience with the system in a routine clinical setting.

METHODS

General Description

The analysis of a patient's diffusion-perfusion mismatch with RAPID is based on diffusion-weighted imaging (DWI) and dynamic susceptibility contrast (DSC) perfusion-weighted imaging (PWI). Specifically, the system has been developed and validated for diffusion-weighted spin-echo echo-planar-imaging (EPI) sequences with and without parallel imaging and with both conventional Stejskal-Tanner and twice-refocused diffusion preparation. Likewise, gradient-echo DSC-MRI EPI scans with and without parallel imaging are compatible with RAPID.

To allow easy and vendor-independent use of RAPID, the software has been packaged in a small form factor computer (6.5" × 6.5" × 10") installed within a hospital network. Serving as an independent DICOM node, the computer communicates directly with MR scanners in the network using a standardized DICOM protocol. The system works as shown on Figure 1. The processing on the RAPID processor is fully automated. Specifically, RAPID computes quantitative diffusion and perfusion parameter maps, segments lesions on these maps, and then derives the mismatch ratio. The results are automatically sent to PACS, to the process-initiating MR scanner, and also to email clients and smartphones upon configuration.

The system was written in C/C++ and leverages on parallel computing to accelerate data processing. Thus, in the current implementation, the processing speed scales linearly with the number of central processing units (CPUs) or CPU cores available. The system currently runs on a Linux operating system (openSuSE 11.2, supported by Novell, Inc., Waltham, MA) with an Intel Core i7 860S 2.53GHz CPU (containing 4 processing cores with hyperthreading which thus allow 8 processing threads to run in parallel) using 4 GB of RAM. The RAPID processing box is connected to the hospital network by means of a gigabit Ethernet link. DICOM compatibility is currently provided by the dcmtk 3.5.4 library (Offis e.V., Oldenburg, Germany). The output image annotation subroutines are currently implemented using MATLAB scripts (MathWorks, Natick, MA) compiled into executable binaries.

The following sections provide a more detailed description of the processing steps (Fig. 2) that define RAPID.

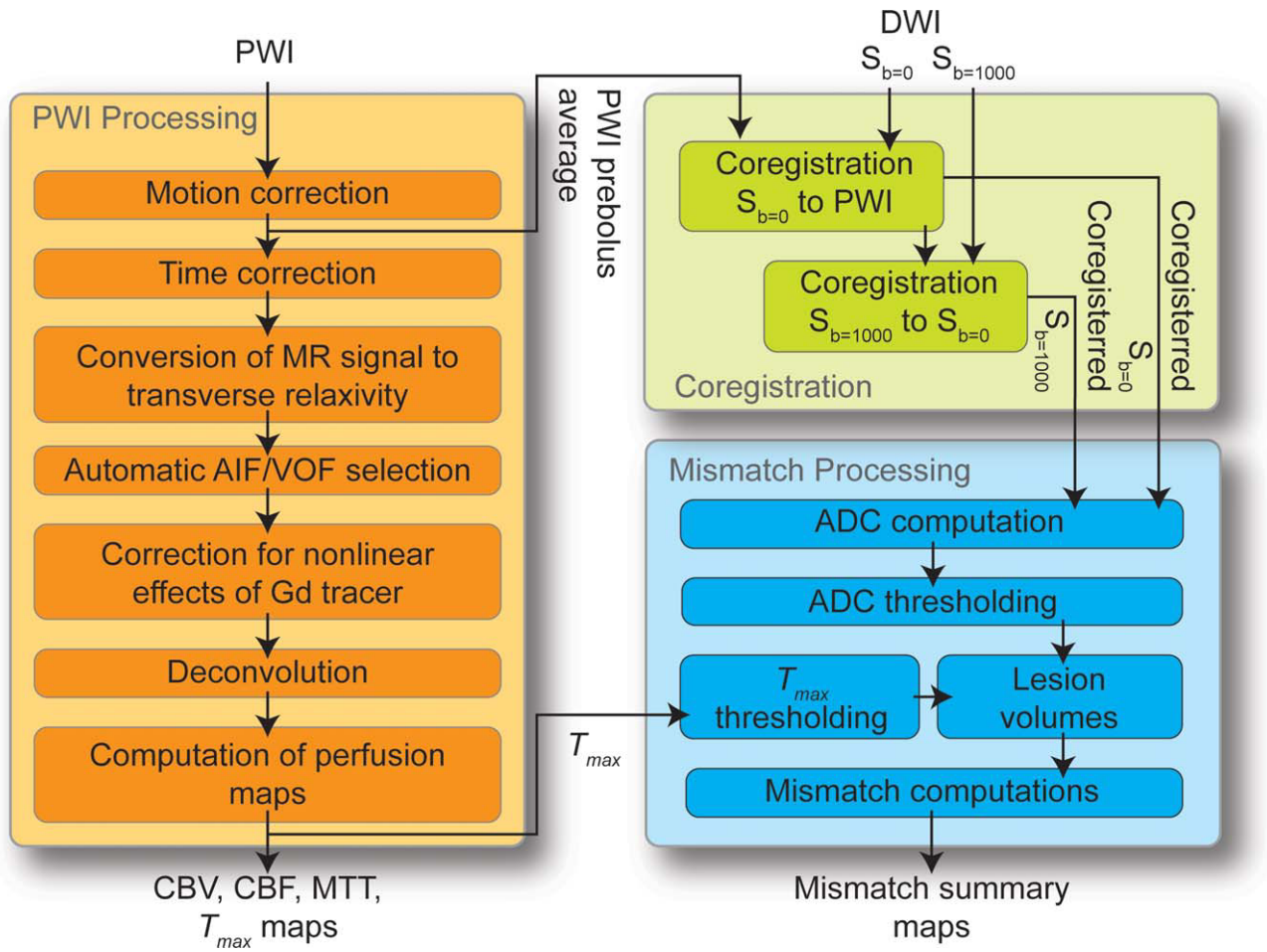

Figure 2. Details of the RAPID pipeline used to calculate mismatch between DWI and PWI. The PWI processing component consists of motion-correction and adjustments for different acquisition times in multi-slice EPI scans, conversion of measured MR signal to estimated changes of transverse relaxivity, automatic detection of AIF and VOF, correction for nonlinear effect of gadolinium tracer in bulk blood and capillaries, deconvolution, and final computation of perfusion parameters. After the PWI processing, DWI $S_{b=0}$ and $S_{b=1000}$ images are spatially coregistered with the PWI data and later resliced to the PWI reference frame. The acute stroke core is identified on ADC maps based on an absolute ADC threshold. Critical hypoperfusion is identified based on T_{max} prolongation beyond a prespecified threshold. Finally, DWI and PWI lesion volumes are determined. The mismatch ratio, as well as the difference in PWI and DWI lesion volumes (estimated penumbra), are computed and included in the output summary. Color figure can be viewed in the online issue, which is available at wileyonlinelibrary.com.

Perfusion

In RAPID, brain regions with altered perfusion are identified on T_{max} maps. Here, the T_{max} parameter is a bolus-shape-independent estimate of time-delay for blood delivery between a main feeding artery (e.g., middle cerebral artery) and tissue at a given spatial location, similar to time-to-peak (TTP) parameter. Although T_{max} and TTP do not directly measure tissue perfusion, they correlate well with hypoperfusion (Fig. 3) based on multiple studies performed by several groups (9–17). It has also been proposed that T_{max} can be used to predict final stroke outcome in patients who do not achieve reperfusion (1,2).

RAPID calculates the quantitative perfusion parameter maps from the acquired DSC-MRI T_2^*-weighted raw perfusion data. The PWI pipeline (Fig. 2) starts by correcting for patient motion using a two-dimensional (2D) in-plane rigid-body registration algorithm. The next step involves correction of slice acquisition times. Typical DSC-MRI acquisitions use single-shot EPI with interleaved slice acquisition, where individual slices are acquired at different time points within the given repetition period. To ensure that signals throughout the whole acquired volume are interpreted equally, RAPID interpolates the signals using b-splines and then resamples them to a common temporal frame-of-reference. This common time base is constructed by taking the time point of the first acquired slice, followed by regularly spaced intervals of the scan repetition period. The b-spline interpolation is used because it allows for resampling of both equidistantly and nonequidistantly sampled PWI data. After time correction, the DSC-MRI signal values are converted to estimates of relative changes in transverse relaxivity. For gradient-echo-based acquisitions this can be expressed as:

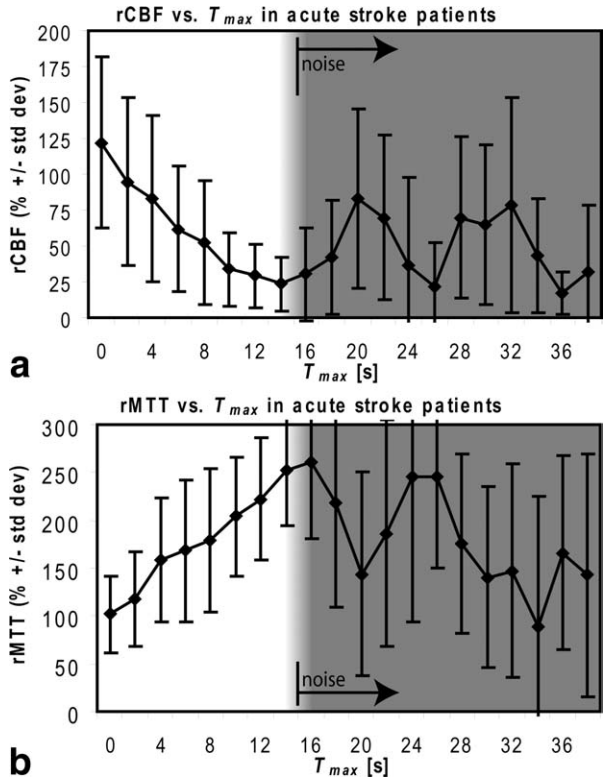

Figure 3. Relation between T_{max}, relative CBF (**a**) and relative MTT (**b**) in acute stroke. The plots suggest that prolonged delay of blood delivery correlates with reduced perfusion in acute stroke. Regions with mild delays in T_{max} ($\leq$6 s) are typically related to delayed flow in deep white matter and watershed regions, or represent regions with benign oligemia, however, delays of 6–14 s are typically related to significant reduction in perfusion. Of note here is that the rCBF and rMTT parameters were obtained by circular, i.e., delay-independent deconvolution. The plots were obtained by analyzing 63 baseline acute stroke cases from DEFUSE trial (1) and averaging results across these datasets. Regions with T_{max} < 4 s were used to determine mean value of normal (i.e., 100%) relative CBF and normal relative MTT. Regions with T_{max} around 0 s mostly represent arteries, hence the relative CBF is above 100%. Regions with T_{max} around 2 s represent proximally fed tissue, whereas regions with T_{max} around 4 s is tissue fed distally or watershed regions. Note that to exemplify the relationship between rCBF, rMTT, and T_{max} in acute stroke, absolute values defining 100% rCBF and rMTT are not important. There is little to no tracer arriving in regions with severely reduced perfusion and thus it is difficult to measure any of the PWI parameters accurately (CBF, MTT, T_{max}). As a result, in regions with apparent T_{max} > 14 s (shaded parts of the plots) the determined CBF and MTT are mostly a noise-induced random values.

$$\Delta R_2^*(t) = -\frac{1}{TE}\log\left(\frac{S(t)}{S_0}\right), \qquad [1]$$

where *S(t)* is the time-resolved MR signal, S_0 is the average of the prebolus (baseline) MR signal after the first few (typically 3) non–steady state time points were discarded, and *TE* is the echo time of the acquisition. Next, RAPID selects locations for both arterial input (AIF) and venous output (VOF) functions in a fully automatic, operator-free manner. RAPID identifies the height, h, arrival time, a, and width, w, of the ΔR_2^* signals at all spatial locations that represent brain tissue or vessels and computes their mean values $\overline{h}$, $\overline{a}$, and $\overline{w}$. Then, the AIF detection algorithm searches for spatially clustered locations with signals of above-average amplitude, below-average width, and early bolus-arrival time to identify possible locations for AIF. Specifically, at a given spatial location, the "fitness" c of a voxel containing a suitable AIF is determined by the following cost function:

$$c = k_1(h - \overline{h}) + k_2(a - \overline{a}) + k_3(w - \overline{w}), \qquad [2]$$

where the weighting coefficients $k_1 = 1.0$, $k_2 = -3.5$, and $k_3 = -1.0$ were optimized empirically by processing 74 PWI datasets from the DEFUSE study (1), as well as other several hundred routine human brain PWI scans. The parameters were optimized for robust delivery of AIF estimates in anatomically appropriate locations (i.e., large arteries of anterior cerebral circulation) under varying sequence parameters, slice prescription, acquisition noise, and bolus shape. The selection algorithm chooses final AIF locations in a region with the highest sum of the spatially clustered values of c. Specifically, we use a cluster of at least three adjacent locations for a pixel size of 1.88 × 1.88 mm and six adjacent locations for a pixel size of 0.94 × 0.94 mm. The selection of the VOF uses a similar algorithm with the assumption of a 3–12 s arteriovenous transit time. For AIF selection, the search is limited to the anterior circulation, whereas for VOF only posterior locations are allowed (i.e., sagittal or transverse sinus). The algorithm currently prefers AIF and VOF locations inside large vessels. Selection of AIF outside of the vessel leads to very complex partial volume effects that can only be corrected with complex-valued data. Such corrections were not considered in the present implementation because the majority of current DSC studies use magnitude MR data only.

Once the locations for both the AIF and the VOF are known, the ΔR_2^* values are converted to estimates of tracer concentration in tissue $c_t(t)$:

$$c_t(t) = x_1 \Delta R_2^*(t) \qquad [3a]$$

and in large vessels (i.e., $c_a(t)$ for AIF and $c_v(t)$ for VOF) as suggested in (18):

$$c_{a,v}(t) = \begin{cases} \frac{-x_2 + \sqrt{x_2^2 + 4x_3\Delta R_2^*(t)}}{2x_3} & \text{for} \quad \Delta R_2^*(t) \geq 0 \\ \frac{x_2 - \sqrt{x_2^2 + 4x_3\Delta R_2^*(t)}}{2x_3} & \text{for} \quad \Delta R_2^*(t) < 0 \end{cases}. \qquad [3b]$$

Values of x_1, x_2, and x_3 are derived from (18), $x_1 = 22.7$ ms.mM, $x_2 = 7.6 \times 10^{-3}$ (ms.mM)$^{-1}$ and $x_3 = 574 \times 10^{-6}$ (ms.mM^2)$^{-1}$ at 1.5 T and $x_1 = 11.5$ ms.mM, $x_2 = 0.493 \times 10^{-3}$ (ms.mM)$^{-1}$ and $x_3 = 2.62 \times 10^{-3}$ (ms.mM^2)$^{-1}$ at 3.0T. Although theoretically $\Delta R_2^* < 0$ is not possible, the quadratic model for estimates of tracer concentration in large vessels (18) does not consider noise possibly present in the signals, and, therefore, to retain zero-mean noise properties, situations with $\Delta R_2^* \geq 0$ and $\Delta R_2^* < 0$ must be treated separately. It has been

speculated that x_1, x_2, and x_3 depend on hematocrit (18,20); however, for the current implementation of RAPID, literature values for hematocrit levels were assumed (18) and were held constant for all subjects. Of course, a deviation in hematocrit level from the assumed value may introduce error into computed blood volume and flow, but the extent of such error was not investigated.

The quantitative perfusion parameters (cerebral blood volume, CBV; cerebral blood flow, CBF; mean transit time, MTT; and the time until the residue function reaches its peak, T_{max}) are obtained by application of a deconvolution method as outlined in literature (3,20–25). Specifically, a circular deconvolution is used which has been shown to provide estimates of the residue functions that are independent from any delays between AIF and bolus arrival in the tissue (25–27). According to indicator-dilution theory, temporally resolved tracer concentrations observed in tissue $c_t(t)$ depend on tissue properties $r(t)$ and the tracer concentration time-course within the vessel that feeds the voxel of interest, $c_a(t)$:

$$c_t(t) = c_a(t) \otimes r(t), \quad [4]$$

where the residue function $r(t) = 1 - h(t)$ represents amount of tracer that remains within tissue capillaries at time t following a hypothetic instantaneous bolus, and $h(t)$ is a distribution function of transit times of the tracer (28). The "$\otimes$" symbol denotes convolution. Of note here is that $r(t)$ allows one to compute bolus-shape independent hemodynamic parameters, and can be determined as:

$$r(t) = c_t(t) \otimes^{-1} c_a(t), \quad [5]$$

where "$\otimes^{-1}$" denotes deconvolution operation. In practice, deconvolution must be regularized (29) to stabilize the solution of $r(t)$ and to produce physically plausible results particularly when the signals to be deconvolved contain noise.

It can be shown that circular deconvolution in the time domain (e.g., using singular value decomposition, SVD) and deconvolution executed in the frequency domain are equivalent (25,27,30). RAPID implements the deconvolution in the frequency domain, as follows:

$$r(t) = \frac{1}{TR} FT^{-1}\left\{ g(f) \frac{C_t(f)}{C_a(f)} \right\}, \quad [6]$$

where

$$C_t(f) = FT\{c_t'(t)\} \quad [7a]$$

and

$$C_a(f) = FT\{c_a'(t)\} \quad [7b]$$

and $c_t'(t)$ and $c_a'(t)$ are the $c_t(t)$ and $c_a(t)$ signals zero-padded to twice their length to avoid time-aliasing (25). TR is the sampling rate, $FT\{\}$ represents the Fourier transform, and f represents frequency, while $FT\{\}^{-1}$ is the inverse Fourier transform. Here, $g(f)$ is a regularization operator:

$$g(f) = \begin{cases} \frac{C_a(f)^2 - N^2}{C_a(f)^2} & \text{if } C_a(f) > N \text{ and } f \neq 0 \\ 1 & \text{if } f = 0 \\ 0 & \text{elsewhere} \end{cases}, \quad [8]$$

where N is an estimate of the noise level of the input signal (23). Because of the nonlinear character of the noise in concentration-related DSC-MRI signals and its dependence on shape and amplitude of the bolus (31), it is difficult to estimate N accurately. Therefore, we applied an approximation approach as proposed in (3,25). Specifically, we define:

$$N = \frac{p_r}{2} . \max \| C_a(f) \|, \quad [9]$$

where p_r is a regularization parameter. The meaning and value of p_r is identical to the regularization parameter proposed previously (3,25). Based on previous works and empirical evidence a value of $p_r = 0.15$ is used. Such regularized deconvolution delivers perfusion estimates that are equivalent to those obtained with block-circulant SVD (25) at 15% regularization level. It is known that selection of the optimal regularization threshold should be governed by noise levels in the DSC-MRI signals, but existing optimization approaches are time consuming and computationally expensive and would prolong delivery of the mismatch analysis results. The intention was also to keep deconvolution algorithm in RAPID as similar as possible to algorithms used in the DEFUSE study (1) to ensure consistency of computed T_{max} values. Application of Wiener-filter-style regularization (Eq. [8]) results in a smoother low-pass filtering than the typically applied sharp box-car-shaped regularization filters (3,25) and thus mitigates oscillatory artifacts in the reconstructed residue function. By formulating the deconvolution problem in the frequency domain, the residue function can be reconstructed with an arbitrary temporal resolution by means of zero-padding (i.e., sinc-interpolation). This allows better estimation of the amplitude and peak position of $r(t)$, and, therefore, improves estimates of CBF and T_{max}. Formulating the deconvolution problem using the Fourier transform also simplifies the application of the Wiener-filter-style regularization. Here, the $f = 0$ component (i.e., the term representing area under the residue curve) must be treated differently in the regularization process from those with $f \neq 0$ (Eq. [8]), to ensure that the CBV computations (which are a scaling factor for the CBF), are unaffected by regularization. Typical SVD-based deconvolution approaches do not allow direct identification of this term, what could contribute to CBF underestimation when combined with Tikhonov regularization (32), which, in this case, is equivalent to Wiener filtering implemented in RAPID.

Next, quantitative perfusion parameters are computed using the following expressions:

$$CBV = 100 \cdot \frac{k_{AV}}{\rho} \frac{(1 - H_{SV})}{(1 - H_{LV})} \frac{\int c_t(t)dt}{\int c_a(t)dt}, \quad [\text{ml}/100\ \text{g}] \quad [10]$$

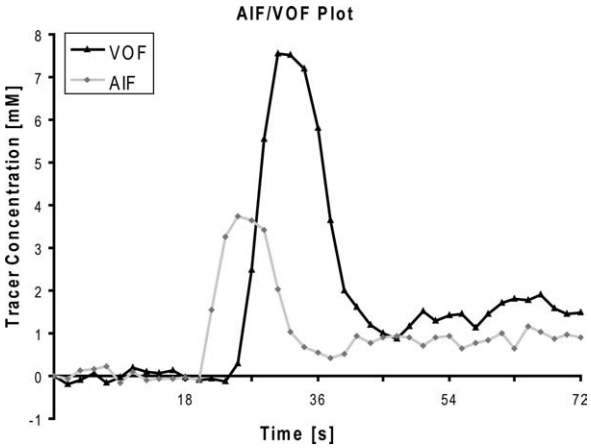

Figure 4. Arterial input (AIF) and venous output (VOF) functions in DSC-MRI. Ideally, the AIF represents the shape of tracer bolus entering the brain. However, the AIF might be scaled due to partial volume effect (PVE). This introduces an unknown confounding factor leading to overestimation of CBV and CBF values. The area under the VOF curve can used to correct for this PVE using Eq. [14]. Note that the peak level of VOF tracer concentration is "clipped" (44) at around 8 mM (usual for acquisition at 1.5T with TE = 40 ms).

$$CBF = 100 \cdot 60 \cdot \frac{k_{AV}}{\rho} \frac{(1 - H_{SV})}{(1 - H_{LV})} [\max(r(t))], \quad [\text{ml}/100\ \text{g}/\text{min}] \quad [11]$$

$$MTT = \frac{60 \cdot CBV}{CBF}, \quad [\text{s}] \quad [12]$$

and

$$T_{\max} = \arg\max_t [r(t)]. \quad [\text{s}] \quad [13]$$

Eqs. [10–13] use infinite integration bounds under the assumption that the analyzed signals: (i) are continuous, (ii) are temporally infinite, (iii) accurately represent concentration of the tracer at each time point, and (iv) have a white noise figure. However, real DSC-MRI measurements are finite and discrete, so the infinite property must be approximated by treating the signals as a single period of an infinite periodic function. The actual implementation of the integration operations is discussed later. Here, max[*r*(*t*)] delivers the maximum value of the residue function *r(t)*, and the function arg max[*r*(*t*)] yields the earliest time t at which this maximum value is detected. Furthermore, H_{SV} and H_{LV} represent a correction for different levels of hematocrit in large vessels and capillaries due to the Fåhreus-Lindquist effect (33,34). Here values of $H_{SV} = 0.25$, $H_{LV} = 0.45$ and $\rho = 1.04$ g/mL (density of the brain) were used as suggested previously (24). Lastly, k_{AV} is a term to correct for partial volume effects (PVE) affecting the AIF:

$$k_{AV} = \frac{\int c_a(t)dt}{\int c_v(t)dt}, \quad [14]$$

where it is expected that $c_v(t)$ is a signal from a vessel large enough not to be subject to PVE. Essentially, k_{AV} is equal to the ratio of areas under AIF and VOF curves (Fig. 4). The use of k_{AV} simply assumes that any PVE in the AIF can be represented by linear scaling. In reality, however, the PVE is very complex and can distort the AIF shape (35). Such shape distortions can affect the computed perfusion parameters. To mitigate the effects of AIF or VOF shape distortions due to high contrast concentration/signal loss during bolus passage, more advanced DSC-MRI acquisition methods such as PERMEATE (36) have been proposed.

In DSC-MRI, the theoretical continuous time-domain signals $c_t(t)$, $c_a(t)$, $r(t)$ are approximated by discrete-time signals $c_t(k)$, $c_a(k)$, $r(k)$ sampled at time points $t_k = k \cdot \text{TR}$ for $k = 0 \,..\, n-1$, where n is number of scan repetitions. In RAPID, the continuous integration $y = \int_{-\infty}^{\infty} x(t)dt$ is approximated by applying circular trapezoidal integration rule. That is, y evaluates to:

$$y = TR \cdot \left\{ \left[\sum_{k=0}^{n-2} \left(\frac{x(k) + x(k+1)}{2} \right) \right] + \left[\frac{x(0) + x(n-1)}{2} \right] \right\}.$$

When modeling the brain perfusion as a linear system and assuming that the blood–brain barrier is intact, it is expected that tracer recirculation will be observed in all $c_a(t)$, $c_v(t)$, and $c_t(t)$ signals. Consequently, using deconvolution and assuming infinitely long scans, the computed estimates of *r(t)* should not be affected by recirculation of the tracer. However, real DSC-MRI measurements are finite and, therefore, delays between arterial, tissue and venous curves will introduce an error into shape and amplitude of the estimated *r(t)*, due to nonidentical lengths of recirculation parts of the curves. A possible solution would be to fit gamma-variate curves to the measured time-concentration signals and thus remove the effect of recirculation, but such approach is time-consuming and might not be sufficiently reliable and accurate. Recirculation can, therefore, have an effect on the accuracy of computed parameters in RAPID. However, with sufficiently long scans, i.e., with scans that sample tracer concentration sufficiently long after the bolus first pass and until a steady concentration of tracer is achieved, the recirculation-induced errors are expected to be smaller than other errors, e.g., those arising from fresh blood inflow (time-of-flight effect) and T_1-shortening effects, etc. that distort the shape of tracer-concentration curves in large vessels. Nevertheless, the extent of error attributable to recirculation and delays was not further investigated.

To alleviate the coarse quantization of $T_{\max}$ values which are typically confined to multiples of the sampling rate *TR*, we zero-pad the regularized *R(f)* to obtain a sinc-interpolated estimate of the residue function *r(t)* with a virtual temporal resolution of 1.0 s. Note that $T_{\max}$ has a significantly reduced dependence on cardiac output and the bolus administration protocol compared with TTP.

Although MR contrast agents have been used for angiographic and perfusion measurements for almost 20 years and are routinely used, it should be noted

that the DSC perfusion acquisition and postprocessing methods presented here rely on off-label use of MR contrast agents.

Diffusion

Diffusion-weighted MRI has been demonstrated to provide a reliable surrogate measure for the infarct core. In particular, the isotropic diffusion-weighted images ($b = 1000$ images) and the diffusion tensor trace maps (the isotropic apparent diffusion coefficient – ADC) have high sensitivity for detecting acute ischemic brain lesions with excellent contrast (37). The $b = 1000$ images ($S_{b=1000}$) are typically preferred by human observers but cannot be used for computerized segmentation. This is because signal hyperintensities in these images can be due to both acute infarct and imaging artifacts, such as susceptibility pile-up, T_2-shine-through, and coil sensitivity field variation. Geometric distortions, etc. can be alleviated by using parallel imaging (SENSE, GRAPPA), however such advanced imaging approaches are not available on every clinical scanner. Moreover, a large number of clinical scans use multi-channel head or head-neck coil arrays. The sum-of-squares reconstruction typically obtained from these coils tend to have much higher signal variation due to the underlying coil sensitivity changes than the bias fields seen on data obtained with quadrature transmit-receive head coils that were most frequently used until a few years ago. The variation of the coil sensitivity (bias field) could be estimated and corrected for by a previous calibration scan, but is often neglected. To mitigate segmentation errors arising from the image artifacts, RAPID uses ADC maps to detect acute stroke lesions, because the bias fields on the $S_{b=1000}$ and $S_{b=0}$ are the same and cancel each other. To compute the ADC maps that are insensitive to patient motion, the DWI data are spatially coregistered with the PWI images (Fig. 2). The prebolus PWI image is used as the static reference image because the PWI images typically have the lowest resolution and consequently are the most susceptible to detrimental resampling artifacts. Here, the $S_{b=0}$ images are aligned with the time-average of the prebolus (baseline) PWI images. The $S_{b=1000}$ images are then aligned with the $S_{b=0}$ data that were already transformed to the PWI reference frame. Then, the realigned $S_{b=1000}$ and $S_{b=0}$ data are resliced into the PWI coordinate space and ADC values are computed as:

$$ADC = -\frac{1}{b}\ln\left(\frac{S_{b=1000}}{S_{b=0}}\right), \quad [\mathrm{mm}^2/\mathrm{s}] \qquad [15]$$

where b is the diffusion weighting factor and $S_{b=0}$ is the signal value when diffusion gradients are turned off.

Lesion Segmentation and Mismatch Computation

Mismatch in RAPID is defined as the ratio between the volume of critically hypoperfused tissue (identified on $T_{\max}$ maps) and the volume of the infarct core (identified on ADC maps). The infarct core is tissue that is deemed irreversibly damaged and which cannot be rescued by reperfusion. The "critically hypoperfused region" refers to tissue that is likely to have critically lowered perfusion, and includes both salvageable (if perfusion is restored early enough) and already irreversibly damaged tissue.

To compute the mismatch between DWI and PWI lesions, the DWI data are first spatially coregistered with the PWI study (Fig. 2) as previously described. The DWI/PWI coregistration also improves robustness of the automated brain tissue segmentation by allowing reliable automated identification of ventricles based on DWI. The ventricles are often difficult to segment from the raw PWI data alone. An example of a coregistered dataset is given in Figure 5.

To exclude nonbrain regions from further segmentation, RAPID forms a brain tissue mask where ADC and prebolus PWI data simultaneously demonstrate valid values. Specifically, ADC values are constrained to lie between 100×10^{-6} mm^2/s and 2100×10^{-6} mm^2/s, whereas for PWI the prebolus signal intensity values must be above 50% of the mean value of the prebolus PWI data obtained by averaging through all voxels in the dataset. As a result, regions representing air, cerebrospinal fluid (CSF) and imaging artifacts (e.g., EPI half field-of-view ghosts) are excluded from further analysis. The masking also excludes locations not covered in both the DWI and the PWI sequences from further analysis.

Ultimately, the stroke core is identified from hypointense regions in ADC maps using an absolute ADC threshold (ADC_{th}). The ADC threshold currently used to identify core is 600×10^{-6} mm^2/s. This threshold was identified with help of a receiver-operator-curve (ROC) analysis that included 32 datasets from the DEFUSE trial (1). Here, we compared prediction of irreversibly damaged and reversibly injured tissue on baseline ADC maps with stroke outcome outlined on 30-day follow-up FLAIR imaging. The analysis was based on an assumption that an optimal ADC threshold for stroke core identification should deliver no false positives outside of the 30-day lesion mask (ignoring contribution from noise), while it should maximize the number of true positives inside the late follow-up lesion. The optimal ADC threshold was chosen as the one that maximized the accuracy of stroke core identification, i.e., the one that showed maximal deviation from the line of no discrimination (Fig. 6) in the ROC plot. The accuracy of the segmentation was rather insensitive to selection of the segmentation threshold ADC_{th} in range from 560×10^{-6} mm^2/s to 640×10^{-6} mm^2/s. ADC_{th} below 560×10^{-6} mm^2/s proved to be insufficiently sensitive, whereas an ADC_{th} above 640×10^{-6} mm^2/s yielded results not specific enough to separate the stroke core from reversible DWI lesions, noise and ADC variations in normal tissue. Details of this analysis will be the subject of a separate publication, but the selected value of $ADC_{th} = 600 \times 10^{-6}$ mm^2/s is in excellent agreement with values available in literature (38,39). The wide plateau on the plot is beneficial as it ensures correctness of segmentation results even under slightly changing

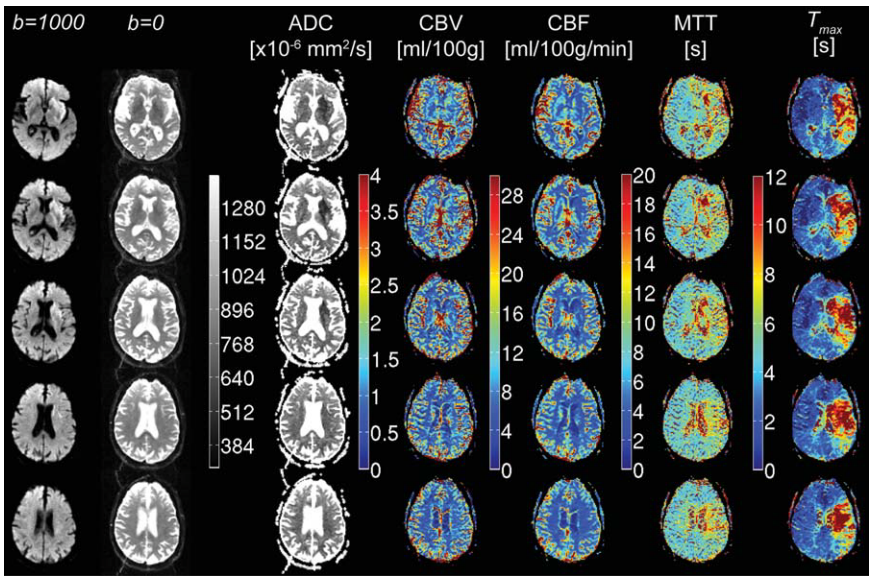

Figure 5. Example of spatially coregistered DWI and PWI datasets. From left to right: $S_{b=1000}$ ("isotropic" diffusion), $S_{b=0}$ (diffusion-weighting gradients turned off = T_2-weighted data), apparent diffusion coefficient (ADC), cerebral blood volume (CBV), cerebral blood flow (CBF), mean transit time (MTT), and T_{max}. The $S_{b=1000}$ and ADC images are used to identify the stroke core, whereas abnormalities on T_{max} and MTT maps indicate hypoperfused tissue. The CBF maps reflect hypoperfusion as well (bottom row), but differences between CBF in gray and white matter and the smaller dynamic range render these maps less conspicuous than maps of temporal perfusion parameters.

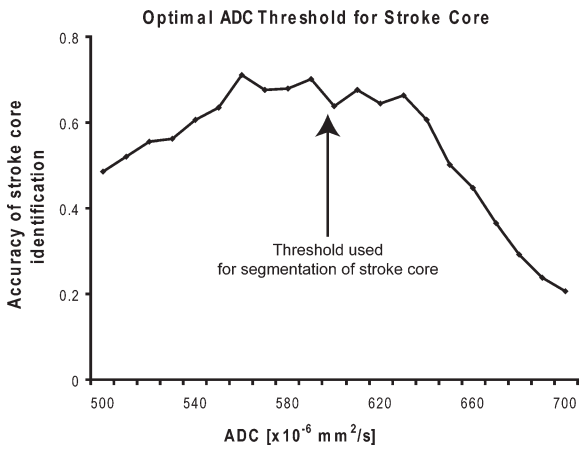

Figure 6.

Figure 6. Accuracy of stroke core identification on baseline ADC versus ADC threshold for the RAPID algorithm. Identification of stroke core lesions in RAPID requires: (i) thresholding of the ADC values and (ii) removal of remaining speckle noise by means of morphological opening operation. This plot depicts the accuracy of stroke core lesion identification after thresholding and morphologic opening as evaluated by ROC analysis. Specifically, the value on vertical axis is the departure of the ROC curve from line of no discrimination (i.e., random guess) for a given ADC threshold. The wide plateau between 560 and 640 $\times$ 10^{-6} mm^2/s is beneficial, as it ensures robustness and accuracy of lesion segmentation even if there are slight changes in imaging parameters such as applied *b*-value or intersubject variation of normal ADC.

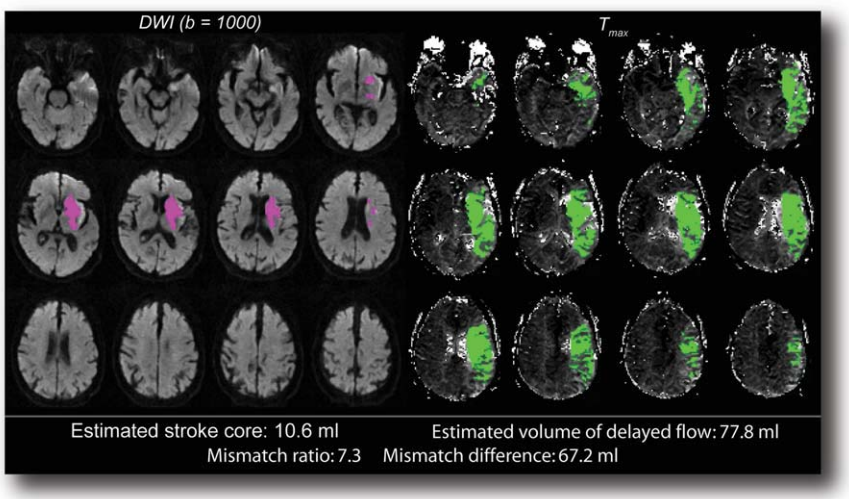

Figure 7. Automatic assessment of DWI/PWI mismatch with RAPID in an acute stroke patient. (Left side) $S_{b=1000}$ images overlaid with stroke core identified using ADC threshold. (Right side) T_{max} maps with green overlay for regions with abnormal flow ($T_{max} > 6$ s). (Bottom) DWI lesion volume, PWI lesion volume, their ratio, and absolute difference is presented. This entire panel is presented automatically to the clinical readers by means of PACS, scanner console, email, and smartphones to facilitate mismatch-based patient triage.

imaging and physiologic parameters that would affect computed ADCs. To make the segmentation robust in presence of noise and imaging artifacts, small objects with the volume below 1 mL were removed from the lesion mask after thresholding the ADC maps.

To segment the abnormal area on PWI, a threshold is applied to identify voxels with $T_{max} > 6$ s. As demonstrated in Figure 3 and as current experience indicates (14,15,17), $T_{max} > 6$ s most accurately estimates critical hypoperfusion, which is beyond what is normally seen due to collateral flow, stenotic feeding vessels or delayed tracer arrival in watershed regions. Based on a virtual sampling rate of 1 s, a $T_{max} > 6$ s is, therefore, used for identifying regions with abnormal flow. For final PWI, lesion outlining small objects with the volume below 3 mL were removed. The noise conditions and imaging artifacts in DSC-MRI are in general worse than in DWI and thus removing small, noise-related objects requires higher thresholds. A typical example of a mismatch assessment in an acute stroke patient is shown on Figure 7.

Evaluation of RAPID

The goal in the development of RAPID was to automatically perform a time-critical assessment of potentially salvageable tissue in acute stroke patients. These data allow the physician to avoid potentially harmful reperfusion therapies in stroke patients with either a malignant profile or little salvageable tissue (1), without the need for a skilled operator to perform PWI and DWI analysis and quantification. Therefore, the system's performance and reliability in predicting mismatch was evaluated and compared with the analysis of the same data by an experienced stroke neurologist or neuroradiologist.

For testing and evaluation purposes, data from the DEFUSE multi-center (7 sites) trial (1) were analyzed. In this trial, single-shot GRE-EPI DSC-MRI perfusion MRI data were acquired at 1.5T whole-body scanners. Depending on make and model, the scan parameters were as follows: TR = 1.4–2.0 s, TE = 40–60 ms, matrix 128^2, field-of-view 24 cm, 12–16 slices (5–7 mm thick separated by gaps of 0–2 mm) to cover the supertentorial brain, and 40–80 time points. A single-dose bolus (0.1 mmol/kg) injection of a gadolinium-based paramagnetic tracer (gadopentetate dimeglumine or gadobenate dimeglumine) was administered typically 10–15 s after the start of the dynamic scan using a MR-compatible power injector followed by 20–25 mL of saline flush at the same flow rate.

In addition to the perfusion MRI data, diffusion-weighted MRI data were also obtained as part of the DEFUSE trial. Specifically, single-shot diffusion-weighted spin-echo EPI scans were acquired with the following scan parameters: TR = 4–6 s, TE = 60–80 ms, matrix 128^2, field-of-view 24 cm, and 12–24 slices (5 mm thick separated by gaps of 0–2 mm). Diffusion-weighted images were acquired with encoding gradients played out separately along the three principal axes at a b-value of 1000 s/mm^2 plus one scan where the diffusion-encoding gradients were turned off ($b = 0$ image), resulting in a total of 4 different diffusion weightings.

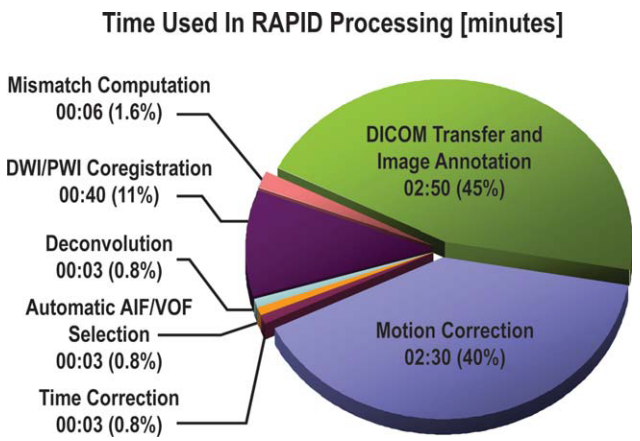

Figure 8. RAPID processing-time benchmark. The majority of the processing time in RAPID is currently spent performing motion correction, DWI/PWI coregistration, DICOM data transfer, and image annotation. The PWI processing algorithms, due to parallelized implementation are not a bottleneck. Total processing time is typically 5–7 min, depending on number of slices, imaging matrix, and severity of patient motion. Color figure can be viewed in the online issue, which is available at wileyonlinelibrary.com.

Thereafter, the three directionally dependent diffusion-weighted images were combined to generate an isotropic diffusion-weighted image ($b = 1000$ image).

The lesion volumes identified by RAPID were compared with those identified by a human reader in 63 of 74 cases, where both DWI and PWI were available and of good diagnostic quality. PWI maps generated by RAPID (that included corrections for motion and different slice times in interleaved-slice EPI acquisitions) were used for both the manual and the automated T_{max} lesion segmentation. Attention was paid by the human reader to check if the AIF used in PWI processing was selected appropriately. Additionally, both methods used identical segmentation criteria (ADC and T_{max} thresholds). RAPID and the human reader used mismatch criteria that were based on the original DEFUSE study (1). A mismatch was considered positive if the difference between the PWI and DWI lesion volume was at least 10 mL and the PWI/DWI volume ratio was at least 1.2. The agreement between diffusion-perfusion-mismatch identified by the human reader and RAPID was analyzed by true positive and false positive rates. Here, the assessment of mismatch by the human reader was considered as ground truth (the "gold standard"). Finally, the inter-reader agreement between the human reader and RAPID was assessed by Cohen's kappa value.

RESULTS

Current Installation Base

For testing and evaluation purposes, RAPID has been integrated into the clinical routine imaging pipeline at our institution. This has allowed processing of more than 2000 cases with PWI and/or DWI abnormalities

in question (15% acute strokes, 30% subacute strokes, 30% cerebral tumors, 10% moya-moya disease, 15% unspecified) between July 2008 and March 2010. The processing of a typical dataset takes currently 5–7 min (Fig. 8), depending on spatial resolution, number of time-points, and possible patient motion. From Figure 8 it is evident that most of the processing time is currently taken up by application of the motion-correction algorithms to PWI time series data before computation of perfusion maps, and also by data transfer and image annotation routines.

RAPID was also selected as tool for immediate evaluation of scan results in two large ongoing clinical trials due to its fully automatic nature, capability to deliver PWI maps and ability to assess mismatch shortly after the MRI scan (DEFUSE2 trial, personal communication with G.W. Albers, Stanford Stroke Center, Stanford, CA, and EXTEND trial, personal communication with S.M. Davis, University of Melbourne, Melbourne, Australia).

For the DEFUSE2 study, RAPID is being tested at following clinical centers: Stanford University Medical Center, Stanford, CA; University of Pittsburgh Medical Center, Pittsburgh, PA, Northwestern Memorial Hospital, Chicago, IL; St. Luke's Hospital, Kansas City, MO; Health Sciences Center, Salt Lake City, UT; Tampa General Hospital, Tampa, FL; University of Texas Southwestern Medical Center, Dallas, TX; Oregon Health Sciences University Hospital, Portland, OR; Queen's Medical Center, Honolulu, HI; Swedish Medical Center, Seattle, WA; Section on Stroke Diagnostics and Therapeutics, National Institute of Neurological Disorders and Stroke (NINDS), National Institutes of Health (NIH), Bethesda, MD; Graz General Hospital, Graz, Austria, and University Hospital, Leuven, Belgium.

In a recent study that compared accuracy of perfusion parameter maps computation using a digital phantom (40), RAPID performed on par with several other academic and commercial perfusion packages. In another study (41), RAPID was found to be as accurate as a human reader in outlining of perfusion lesions on T_{max} maps.

Comparison of Automated and Manual Segmentation of Lesion Volumes and Mismatch Identification

Results for the 63 cases analyzed both manually and with RAPID are presented in Figure 9. The correlation between DWI lesion volumes using the manual and the automatic approach was $r^2 = 0.99$ (Fig. 9a). The slope of the regression line was 0.99 and its intercept value was −0.05. The correlation between PWI lesion volumes using the manual and the automatic method was $r^2 = 0.96$ (Fig. 9b). The slope of the regression line was 1.11 and its intercept value was −0.99. Note that the automatic method was sensitive only to objects of size above 1 mL for DWI and above 3 mL for PWI due to the thresholding operation applied for robustness to noise and image artifacts.

The diffusion-perfusion-mismatch identified by RAPID was in agreement with the observation of a human reader in 60 cases (95.2%) and in disagreement in 3 cases (4.8%, 3 false positives). Specifically, the agreement in mismatch assessment between the human reader and RAPID, as assessed by Cohen's kappa, was $\kappa = 0.90$. RAPID was able to identify mismatch with 100% sensitivity and 91% specificity (false positive rate = 9.1%, false negative rate = 0%) in analysis with observations of the human reader as a ground truth. Note, however, that the segmentation criteria used for the identification of stroke core (ADC $< 600 \times 10^{-6}$ mm^2/s) and critically hypoperfused tissue ($T_{max} > 6$ s @ 1 s sampling resolution) were different from those used in the DEFUSE trial (1) ($S_{b=1000} > \text{mean}(S_{b=1000}) + 3.0 \times \text{SD}(S_{b=1000})$; $T_{max} > 4$ s @ 1.4–2.0 s sampling resolution) and reflect recent advances and adjustments for robust automated lesion identification.

DISCUSSION

We have developed a novel system to perform real-time, fully automated identification of diffusion-perfusion mismatch in acute stroke patients. This system has been deployed at our institution on five 1.5T and three 3.0T scanners and integrated into the routine diagnostic pipeline where it currently processes 6–10 cases per day. The system processes all clinical cases performed with DWI and GRE-EPI DSC-MRI acquisitions. Although not validated, echo-shifted SSFP sequences (such as PRESTO) and diffusion-weighted FSE sequences (such as PROPELLER) have been also successfully processed using the RAPID pipeline. RAPID is also the processing tool used in two large acute stroke trials that are currently underway (DEFUSE2, EXTEND) and this manuscript should serve as a future reference basis for the processing methods used in these trials.

Currently, one case is processed in approximately 5–7 min, depending in part on the hardware platform on which RAPID is implemented. RAPID could easily be installed on a more powerful machine; however, a small form factor computer was chosen for the present implementation to save space in the usually very tight MR control rooms. For example, one case can be processed in 1:30 min on a current state-of-the art Intel Xeon E5570 or AMD Opteron 8378 based platform with 16 CPU cores processing data threads in parallel. Although RAPID requires a separate dedicated computer, no additional training is required for neuroradiologists and other clinicians, and the processed data are readily available in PACS.

To benchmark and to evaluate RAPID, a large number of research datasets were processed and analyzed. The system was tested across a wide range of imaging parameters and variable data quality. It has been demonstrated that RAPID is robust and accurate enough for a reliable identification of diffusion-perfusion mismatch. The differences in PWI and DWI volumes identified by manual and automatic approaches (Fig. 9) can be attributed to two main factors. First, a human reader could ignore certain imaging artifacts that the automatic segmentation could not, leading to

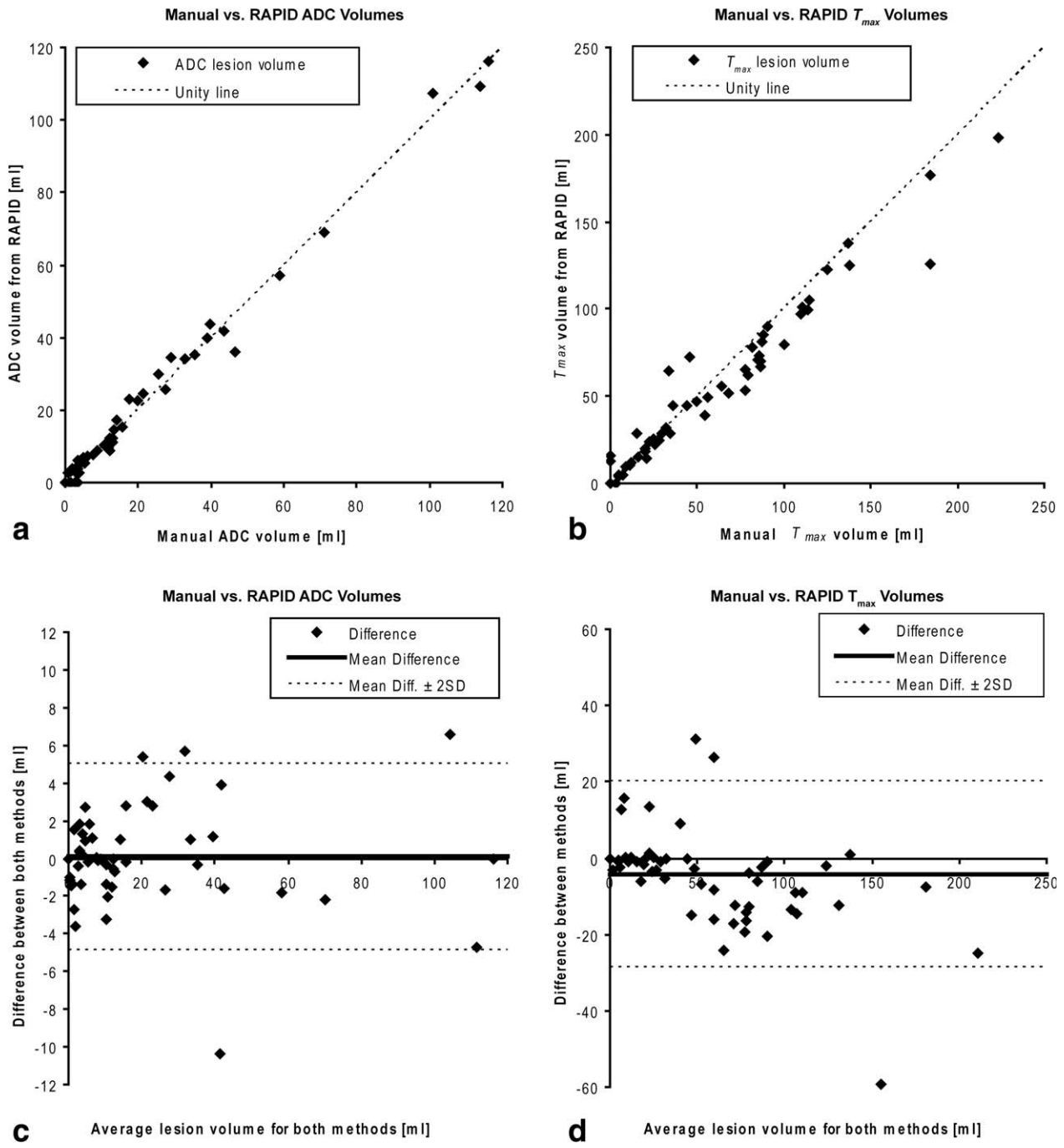

Figure 9. Comparison of stroke core and hypoperfused region volumes identified by a human reader and by RAPID. Correlation between manual and automated methods for determining stroke core volume on ADC maps (**a**) and volumes of hypoperfused tissue on T_{max} (**b**). Difference between the methods with respect to mean of the results (Bland-Altman plots), for stroke core on ADC maps (**c**) and hypoperfused tissue on T_{max} (**d**).

overestimation of volumes by RAPID. Second, the automated processing ignored parts of DWI or PWI lesions present in locations not covered by both DWI and PWI scans (e.g., cerebellum), which led to underestimation of volumes in automatic assessment compared with results of the human reader. The false positive identification of mismatch was caused by imaging artifacts in the raw PWI data sets, particularly, through-plane patient motion and susceptibility-induced signal loss. These artifacts caused regions with artificially high T_{max} that were erroneously added to the segmented lesion, thus increased the segmented lesion volumes. The majority of the discrepancies in segmentation and mismatch assessments can be attributed to data quality; however, this was mainly a problem with earlier existing data from the DEFUSE study. Forthcoming studies using better imaging techniques and optimized imaging protocols

will have better data quality and fewer confounding artifacts. Nevertheless, even in the original DEFUSE patients, the automated processing delivered suboptimal results for only 3 of 63 cases.

Certainly, as with any computer method, the overall robustness of the system highly depends on the quality of input DWI and PWI data, and can be easily degraded by patient motion or scanner hardware failure. In our experience, around 10% of acute stroke datasets tend to be corrupted by strong motion. Therefore, the system implements multiple measures to correct for patient motion or to become insensitive to signal changes induced by motion. Nevertheless, motion continues to be a problem even in manual data processing, because heavy through-plane motion cannot currently be corrected sufficiently with retrospective methods. Fortunately, there are several ways to identify cases corrupted by motion. First, the presence of motion artifacts can be ascertained from raw PWI data available in PACS. Second, the motion can be detected by computerized methods and the cost functions used for image registration can be used to directly derive an image quality indicator as well as a metric for successful registration. The intrinsic vulnerability to out-of-plane motion of the 2D acquisition methods used in DSC-MRI could be addressed by prospective motion-correction methods, however few vendors currently provide such capability and these methods are not yet ready for routine clinical use.

RAPID currently identifies the ratio between the volume of the infarct core and the volume of the hypoperfused tissue, also known as the volumetric mismatch. Recent studies indicate that mismatch can alternatively be defined as *coregistered mismatch*—that is the voxel-wise mismatch between core and penumbra (42). Even though RAPID is capable of computing this mismatch measure, it is not used in the current approach because of concerns that coregistration inaccuracies combined with imaging artifacts, such as EPI distortions, strongly influence the results. Nevertheless, the coregistered mismatch warrants further investigation.

Although RAPID has fulfilled a previously unmet clinical need, work is ongoing to improve several aspects of the system. First, the system currently uses an absolute ADC threshold and thus might be inaccurate for subacute strokes where ADC pseudonormalizes (43). Second, the T_{max} does not reflect blood flow directly. For example, prolonged T_{max} can be caused by stenotic vessels or collateral flow as well. Still, in our experience, in acute stroke the prolonged T_{max} correlates well with lowered CBF (Fig. 3). Third, the computed CBV and CBF values are not absolute. This is due to the known nonlinearities (18,35) and errors in MR PWI signal acquisitions and is predominantly caused by inaccuracies in the estimation of contrast agent concentration in large vessels providing the AIF and VOF. Here, the challenges are signal peak clipping (44), fast flow of blood in large vessels, T_1-effects (45), unknown hematocrit and the dependency of the tracer effect on vessel orientation relative to the main magnetic field (18,19,46,47). Signal peak clipping is known to cause errors in CBV and CBF estimation (48), but has much less effect on T_{max}. T_{max} is also independent of the area under the VOF (Eq. [13]). Furthermore, according to our simulations (unpublished data), T_{max} estimates generally remain quite unaltered even when AIF amplitude is changed by clipping, particularly when regularized deconvolution is used. The low-pass filtering in the regularization limits the effect of clipping to a change in AIF amplitude only, and hence has little to no effect on T_{max} computation. However, this effect certainly depends on the shape of the bolus curve and dosage of the tracer and should be investigated in future studies. Existing artifacts in DSC-MRI signal can be addressed by using multi-echo acquisitions (36) and using the MR signal phase instead of signal magnitude for tracer concentration computation, but these methods are not widely available yet and, therefore, we tested RAPID only with conventional DSC-PWI data. Fourth, if the blood–brain barrier is not intact in certain regions, the PWI computation might deliver inaccurate results of CBV, CBF, and MTT maps due to extravasation of the contrast agent. In future revisions, these effects will be modeled using existing approaches (49) and thus potentially improve the accuracy of the PWI parameter estimation.

The results of this work indicate that automatic processing of DWI and PWI in RAPID is sufficiently fast for identification of the mismatch in an acute stroke setting and is comparable to manual lesion outlining. The failure rate of RAPID is very low and in our experience it has been outweighed by the convenience of having immediate information about diffusion-perfusion mismatch without the subjectivity of a human operator. In addition to the mismatch assessment, the system also provides CBV, CBF, MTT, and T_{max} maps which are extremely valuable to the stroke treatment team in their daily routine. Stroke neurologists, neuroradiologists, and residents consider the system to be extremely useful and a valuable addition to routine PWI and acute stroke patient workup.

ACKNOWLEDGMENTS

The authors thank Dr. Maarten G. Lansberg, Dr. Greg Zaharchuk, Dr. Michael Mlynash, Dr. Søren Christensen, Dr. Jean-Marc Olivot, and Dr. Deidre A. De Silva for valuable input during the multiple phases of development and evaluation of RAPID. The authors also thank Dr. Rafael O'Halloran for proofreading the manuscript. Finally, the authors thank all DEFUSE and EPITHET investigators for providing data as well as all DEFUSE2 and EXTEND investigators for evaluating RAPID and providing feedback. The authors also express special gratitude to Don Valentine. Without his constant support and encouragement this project would have never been possible.

REFERENCES

1. Albers GW, Thijs VN, Wechsler L, et al. Magnetic resonance imaging profiles predict clinical response to early reperfusion: the

diffusion and perfusion imaging evaluation for understanding stroke evolution (DEFUSE) study. Ann Neurol 2006;60: 508–517.
2. Davis SM, Donnan GA, Parsons MW, et al. Effects of alteplase beyond 3 h after stroke in the echoplanar imaging thrombolytic evaluation trial (EPITHET): a placebo-controlled randomised trial. Lancet Neurol 2008;7:299–309.
3. Østergaard L, Weisskoff RM, Chesler DA, Gyldensted C, Rosen BR. High resolution measurement of cerebral blood flow using intravascular tracer bolus passages. Part I. Mathematical approach and statistical analysis. Magn Reson Med 1996;36: 715–725.
4. Mouridsen K, Christensen S, Gyldensted L, Ostergaard L. Automatic selection of arterial input function using cluster analysis. Magn Reson Med 2006;55:524–531.
5. Kosior JC, Frayne R. PerfTool: a software platform for investigating bolus-tracking perfusion imaging quantification strategies. J Magn Reson Imaging 2007;25:653–659.
6. Rose SE, Chalk JB, Griffin MP, et al. MRI based diffusion and perfusion predictive model to estimate stroke evolution. Magn Reson Imaging 2001;19:1043–1053.
7. Perfusion Mismatch Analyzer, version 3.0.0.0. ASIST-Japan Web site. Available at: http://asist.umin.jp/index-e.htm. Published November 2006, updated February 2009. Accessed February 20, 2009.
8. Kudo K, Sasaki M, Momoshima S, Yamada K, Terae S, Shirato H. Development of perfusion mismatch analyzer (PMA): fully automated, operator-independent and standardized PWI-DWI analysis software. In: Proceedings of the 93rd Annual Meetings of RSNA, Educational Exhibit 2007, LL-NR3212.
9. Kidwell CS, Saver JL, Mattiello J, et al. Diffusion-perfusion MR evaluation of perihematomal injury in hyperacute intracerebral hemorrhage. Neurology 2001;57:1611–1617.
10. Wintermark M, Reichhart M, Cuisenaire O, et al. Comparison of admission perfusion computed tomography and qualitative diffusion- and perfusion-weighted magnetic resonance imaging in acute stroke patients. Stroke 2002;33:2025–2031.
11. Kidwell CS, Alger JR, Saver JL. Beyond mismatch: evolving paradigms in imaging the ischemic penumbra with multimodal magnetic resonance imaging. Stroke 2003;34:2729–2735.
12. Shih LC, Saver JL, Alger JR, et al. Perfusion-weighted magnetic resonance imaging thresholds identifying core, irreversibly infarcted tissue. Stroke 2003;34:1425–1430.
13. Wintermark M, Flanders AE, Velthuis B, et al. Perfusion-CT assessment of infarct core and penumbra receiver operating characteristic curve analysis in 130 patients suspected of acute hemispheric stroke. Stroke 2006;37:979–985.
14. Olivot JM, Mlynash M, Zaharchuk G, et al. Perfusion MRI (Tmax and MTT) correlation with xenon CT cerebral blood flow in stroke patients. Neurology 2009;72:1140–1145.
15. Olivot JM, Mlynash M, Thijs VN, et al. Optimal Tmax threshold for predicting penumbral tissue in acute stroke. Stroke 2009;40: 469–475.
16. Takasawa M, Jones PS, Guadagno JV, et al. How reliable is perfusion MR in acute stroke? Validation and determination of the penumbra threshold against quantitative PET. Stroke 2008;39: 870–877.
17. Christensen S, Mouridsen K, Wu O, et al. Comparison of 10 perfusion MRI parameters in 97 sub-6-hour stroke patients using voxel-based receiver operating characteristics analysis. Stroke 2009;40:2055–2061.
18. Kjølby BF, Østergaard L, Kiselev VG. Theoretical model of intravascular paramagnetic tracers effect on tissue relaxation. Magn Reson Med 2006;56:187–197.
19. Conturo TE, Akbudak E, Kotys MS, et al. Arterial input functions for dynamic susceptibility contrast MRI: requirements and signal options. J Magn Reson Imaging 2005;22:697–703.
20. Meier P, Zierler KL. On the theory of the indicator-dillution method for measurement of blood flow and volume. J Appl Physiol 1954;6:731–744.
21. Zierler KL. Theoretical basis of indicator-dilution methods for measuring flow and volume. Circ Res 1962;10:393–407.
22. Axel L. Cerebral blood flow determination by rapid-sequence computed tomography. Radiology 1980;137:679–686.
23. Gobbel GT, Fike JR. A deconvolution method for evaluating indicator-dilution curves. Phys Med Biol 1994;39: 1833–1854.
24. Rempp KA, Brix G, Wenz F, Becker CR, Gückel F, Lorenz WJ. Quantification of regional cerebral blood flow and volume with dynamic susceptibility contrast-enhanced MR imaging. Radiology 1994;193:637–641.
25. Wu O, Østergaard L, Weisskoff RM, Benner T, Rosen BR, Sorensen AG. Tracer arrival timing-insensitive technique for estimating flow in MR perfusion-weighted imaging using singular value decomposition with a block-circulant deconvolution matrix. Magn Reson Med 2003;50:164–174.
26. Calamante F, Gadian DG, Connelly A. Delay and dispersion effects in dynamic susceptibility contrast MRI: simulations using singular value decomposition. Magn Reson Med 2000;44: 466–473.
27. Gall P, Emerich P, Kjølby BF, Kellner E, Mader I, Kiselev VG. On the design of filters for fourier and oSVD-based deconvolution in bolus tracking perfusion MRI. Magn Reson Mater Phys 2010;23: 187–195.
28. Weisskoff RM, Chesler D, Boxerman JL, Rosen BR. Pitfalls in MR measurement of tissue blood flow with intravascular tracers: which mean transit time? Magn Reson Med 1993;29: 553–558.
29. Hansen PC. Rank-deficient and discrete ill-posed problems. Numerical aspects of linear inversion, 1st edition. Philadelphia: Society of Industrial And Applied Mathemathics (SIAM); 1998. 247 p.
30. Alsop D, Schlaug G. The equivalence of SVD and Fourier deconvolution for dynamic susceptibility contrast analysis. In: Proceedings of 9th Annual Meeting of ISMRM, Glasgow, Scotland, 2001. (abstract 1581).
31. Smith MR, Lu H, Frayne R. Signal-to-noise ratio effects in quantitative cerebral perfusion using dynamic susceptibility contrast agents. Magn Reson Med 2003;49:122–128.
32. Calamante F, Gadian DG, Connelly A. Quantification of bolus-tracking MRI: improved characterization of the tissue residue function using Tikhonov regularization. Magn Reson Med 2003; 50:1237–1247.
33. Fåhreus R, Lindquist T. The viscosity of the blood in narrow capillary tubes. Am J Physiol 1931;96:562–568.
34. Chacalos EH. Variations in small and large vessel volumes caused by cations, adrenaline and histamine. J Physiol 1967; 188:141–158.
35. van Osch MJP, van der Grond J, Bakker CJG. Partial volume effects on arterial input functions: shape and amplitude distortions and their correction. J Magn Reson Imaging 2005;22: 704–709.
36. Newbould RD, Stefan ST, Jochimsen TH, et al. Perfusion mapping with multiecho multishot parallel imaging EPI. Magn Reson Med 2007;58:70–81.
37. Schaefer PW, Copen WA, Lev MH, Gonzalez RG. Diffusion-weighted imaging in acute stroke. Neuroimaging Clin N Am 2005; 15:503–530.
38. Kidwell CS, Saver JL, Starkman S, et al. Late secondary ischemic injury in patients receiving intraarterial thrombolysis. Ann Neurol 2002;52:698–703.
39. Schaefer PW, Hunter GJ, He J, et al. Predicting cerebral ischemic infarct volume with diffusion and perfusion MR imaging. AJNR Am J Neuroradiol 2002;23:1785–1794.
40. Kudo K, Christensen S, Sasaki M, et al. Accuracy and reliability of post-processing software for DSC MR perfusion: quantitative analysis by digital phantom data. In: Proceedings of the 18th Annual Meeting of the ISMRM, Stockholm, Sweden, 2010. (abstract 4990).
41. Christensen S, Campbell BC, de la Ossa NP, et al. Optimal perfusion thresholds for prediction of tissue destined for infarction in the combined EPITHET and DEFUSE dataset. In: International Stroke Conference Poster Presentations, Proceedings of the International Stroke Conference, San Antonio, TX, USA, 2010. Stroke 2010:41. Poster P164. Available on-line at http://stroke.ahajournals.org.
42. Ma H, Zavala JA, Teoh H, et al. Penumbral mismatch is underestimated using standard volumetric methods and this is exacerbated with time. J Neurol Neurosurg Psychiatry 2009;80: 991–997.
43. Bammer R, Stollberger R, Augustin M, et al. Diffusion-weighted imaging with navigated interleaved echo-planar imaging and a conventional gradient system. Radiology 1999;211: 799–806.

44. Ellinger R, Kremser C, Schocke MFH, et al. The impact of peak saturation of the arterial input function on quantitative evaluation of dynamic susceptibility contrast-enhanced MR studies. J Comput Assist Tomogr 2000;24:942–948.
45. Calamante F, Vonken EPA, van Osch MJP. Contrast agent concentration measurements affecting quantification of bolus-tracking perfusion MRI. Magn Reson Med 2007;58: 544–553.
46. Kiselev VG. On the theoretical basis of perfusion measurements by dynamic susceptibility contrast MRI. Magn Reson Med 2001; 46:1113–1122.
47. van Osch MJP, Vonken EPA, Viergever MA, van der Grond J, Bakker CJG. Measuring the arterial input function with gradient echo sequences. Magn Reson Med 2003;49:1067–1076.
48. Knuttson L, Börjesson S, Larsson EM, et al. Absolute quantification of cerebral blood flow in normal volunteers: correlation between Xe-133 SPECT and dynamic susceptibility contrast MRI. J Magn Reson Imaging 2007;26:913–920.
49. Boxerman JL, Schmainda KM, Weisskoff RM. Relative cerebral blood volume maps corrected for contrast agent extravasation significantly correlate with glioma tumor grade, whereas uncorrected maps do not. AJNR Am J Neuroradiol 2006;27:859–867.